Study on Added Resistance with Measured Unsteady Pressure Distribution on Ship-hull Surface

Masashi Kashiwagi[*], **Hidetsugu Iwashita**[**],
Soma Miura[*] **and Munehiko Hinatsu**[*]

[*] Dept of Naval Architecture & Ocean Engineering, Osaka University, Japan
[**] Dept of Transportation & Environmental Systems, Hiroshima University, Japan

E-mail: kashi@naoe.eng.osaka-u.ac.jp

1 INTRODUCTION

With increase in the demand for accurate prediction of the propulsion performance of a ship in actual seas, much research interest is recently focused on the added resistance in waves. However, no enhancement in our hydrodynamic understanding would be achieved, if comparisons between experimental measurement and numerical computation would be made only for the integrated total force. We need to study on the spatial distribution of unsteady pressure on the ship-hull surface, especially the distribution of second-order added pressure and the resultant distribution of time-averaged steady force in the longitudinal direction of a ship. Experimental measurement of this kind of added-pressure distribution is difficult and hence has not been conducted so far.

For this challenging work, we have used a large number of FBG (Fiber Bragg Gratings) pressure sensors[1] and obtained for the first time the spatial distribution of unsteady pressure on the ship-hull surface. However, in the experiment conducted in 2017, the number of sensors affixed above the still waterline was insufficient to obtain a reliable result for the added-pressure distribution. Thus after some preliminary check and improvement of the FBG sensor, we have conducted the measurement again in 2018 by using 333 FBG sensors affixed only on the port side of a ship, among which 70 sensors were placed above the still waterline. Repeatability and accuracy is confirmed in obtained results for the first harmonic component of the unsteady pressure through comparison with corresponding results obtained in 2017. Then a study is made in this paper on the added-pressure distribution and which part of a ship is predominant in the added resistance.

2 FBG PRESSURE SENSOR

The mechanism and measurement principle of the FBG pressure sensor is the same as that introduced last year[1]. Namely, in the FBG only a particular wavelength of light (called Bragg wavelength) will be reflected by the distributed diffraction grating etched in the optical fiber core. If the spacing between reflectors changes due to variation of pressure load or temperature, the Bragg wavelength also changes. Thus by identifying a change in the Bragg wavelength in terms of a calibration factor obtained beforehand, the pressure can be measured.

We have tried to improve reliability of the sensor, minimizing the effect of temperature variation on the pressure to be measured and the size of the sensor itself, but the FBG sensor eventually

Fig. 1 FBG sensor.

used in 2018 was almost the same as that used in 2017. Fig. 1 shows a schematic diagram of the FBG sensor used, with 9 mm in diameter, 15 mm in length, and 0.6 mm in thickness. One sensor can measure the pressure and temperature at the same time, because two FBGs with different spacings of Bragg grating are contained in one sensor and fixed in order not to interfere with each other. Therefore, the effect of temperature variation on the pressure measurement can be compensated.
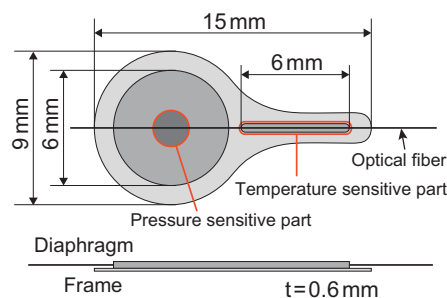
3 EXPERIMENTAL MEASUREMENT IN 2018

The experiment was conducted in September 2018 at the towing tank of RIAM (Research Institute for Applied Mechanics), Kyushu University, using the same ship model as that in previous years, i.e. the RIOS bulk carrier[1,2] of $C_B = 0.8$. Fig. 2 depicts the position of pressure sensors in the experiment in 2018. Since we
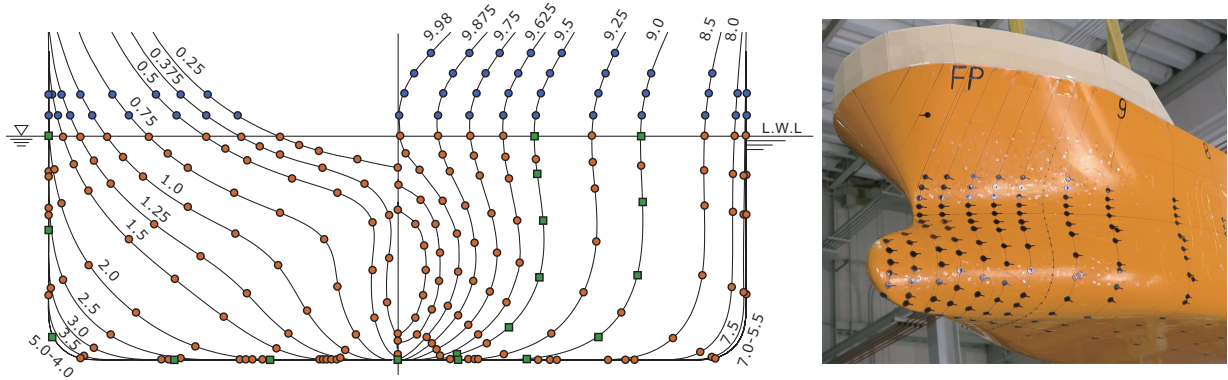
Fig. 2 Position of pressure sensors attached on RIOS bulk carrier.

realized in the experiment in 2017 that more sensors need to be placed above the still waterline to enhance our understanding of hydrodynamic nature in the added resistance, we used totally 333 FBG pressure sensors including 70 sensors above the still waterline; which were affixed on the port side as shown in Fig. 2, and 19 strain-type pressure sensors were embedded in the starboard side (at ordinate numbers 5.0, 9.0, and 9.5, indicated by green-color square symbol in Fig. 2) to check the measurement accuracy of the FBG pressure sensors. The measurement has been done at Fn = 0.18 in head waves of λ/L = 0.3, 0.4, 0.5, 0.8, 1.0, 1.25, 1.5, and 2.0. In addition to the pressure measurement, we measured the wave-induced ship motions and the total added resistance by means of a dynamometer mounted on the lowest part of a heaving rod in the motion measurement device. Furthermore, both steady and unsteady wave profiles on the ship-hull surface were measured in 2018 using capacitance-type wave gauges set at some transverse sections and along the hull surface with small separation gap.

4 NUMERICAL CALCULATIONS

In order to see the degree of agreement (or limitation) of the potential-flow computation methods, the measured unsteady pressure distribution is compared with computed values by EUT (Enhanced Unified Theory) developed by Kashiwagi[3] and by RPM (Rankine Panel Method) developed by Iwashita et al[4]. Furthermore, to understand nonlinear behavior in the unsteady pressure and resultant added resistance especially near the free surface, a CFD commercial software FINE/Marine is also used.

5 RESULTS AND DISCUSSION

5.1 First-harmonic Pressure Distribution

In order to see repeatability, accuracy, and nonlinearity in measured results, an example of the result is shown in Fig. 3 for λ/L = 0.5 of head wave and Fn = 0.18; in which the measured values with improved FBG sensors in 2018 are compared to the values with FBG sensors in 2017 and also to the values with strain-type pressure
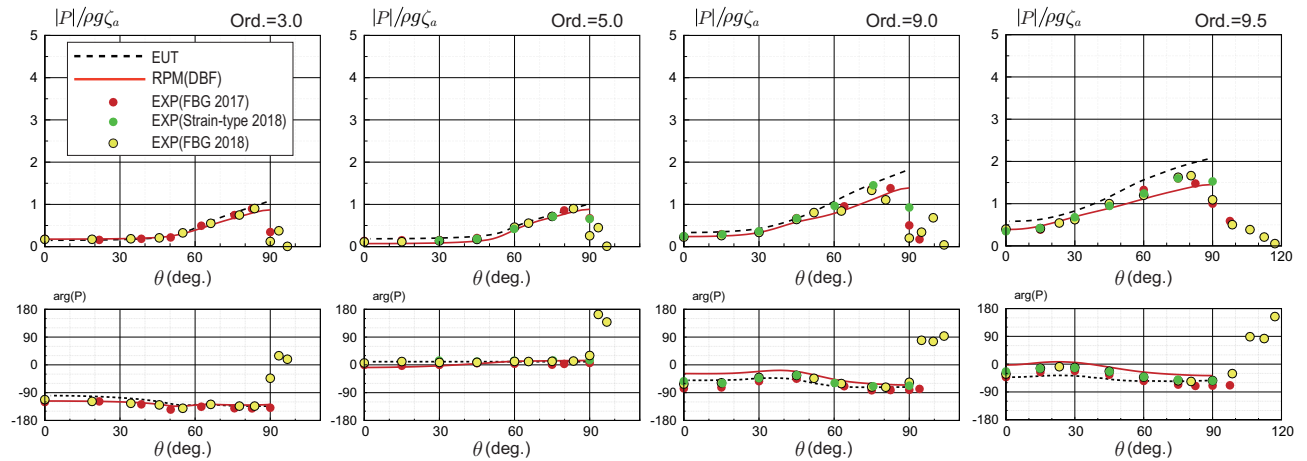

Fig. 3 Sectional unsteady pressure distribution at Fn = 0.18, χ = 180 deg, and λ/L = 0.5.

sensors in 2018 mounted at ordinate numbers 5.0, 9.0, and 9.5. The abscissa θ indicates the location of sensors in the polar angle, with $\theta = 0$ deg being the centerline on the bottom and $\theta = 90$ deg the still waterline. (We note that there are more measured data in 2018 above the still waterline of $\theta > 90$ deg.) The agreement among these measured values is acceptable, confirming repeatability and accuracy in measured results by FBG sensors. Computed results by EUT and RPM are also shown with broken and solid lines, respectively, and the agreement of these computed results with measured values is also favorable except for a nonlinear region around $\theta = 90$ deg, where the time history of measured pressures takes a half-rectified nonlinear profile but is analyzed directly using the Fourier-series decomposition without any correction.

5.2 Added Pressure and Added Resistance

The added resistance can be computed from the difference between the time-averaged second-order force in waves and the resistance at steady translation of a ship in calm water. Likewise, the added pressure is defined as the difference of the steady pressures in calm water and in waves. When a ship is oscillating in waves, the difference in the normal vector on the ship hull between the space-fixed and body-fixed coordinate systems must be taken into account, which can be given by Taylor expansion as follows:

$$N = n + \alpha_R \times n + [H]n + \cdots \tag{1}$$

where n means the normal vector in the body-fixed coordinate system, α_R the first-order rotational-motion vector, and $[H]$ the second-order matrix to be obtained by Taylor expansion of the Euler-angle matrix. Suppose that the pressure is given as a sum of the zeroth-order steady pressure $p^{(0)}(x)$ due to steady translation of a ship in calm water, the first-order oscillatory pressure $p^{(1)}(x)$ in wave, and the second-order time-averaged pressure $p^{(2)}(x)$ in wave. Then, the added pressure is defined as $p_{AW}^{(2)}(x) = p^{(2)}(x) - p^{(0)}(x)$. In terms of Eq. (1), by definition, the added resistance can be computed in the form

$$R_{AW} = \iint_{S_H} \left\{ p_{AW}^{(2)}(x)\, n_x + \overline{p^{(1)}(x)\left(\alpha_R \times n\right)_x} + \overline{p^{(0)}(x)\left([H]n\right)_x} \right\} dS \tag{2}$$

where S_H denotes the wetted surface of a ship, and the overbar means the time average to be taken. We note that the effect of steady trim is neglected in Eq. (2).

In this paper, the contributions from the second and third terms in Eq. (2) are neglected and then, the added resistance is computed only from integration of the added pressure. Namely,

$$R_{AW} \simeq \iint_{S_H} p_{AW}^{(2)}(x)\, n_x\, dS = \sum_{j=1}^{NH} p_{AW,j}^{(2)}\, S_j\, n_{x,j} \tag{3}$$

where $j = 1 \sim NH$ denotes the number of discretized panels on the ship-hull surface, $p_{AW,j}^{(2)}$ the value of added pressure at the center of j-th panel, and $S_j n_{x,j}$ the product of the area and the x-component of the normal vector on the j-th panel.

Fn=0.18, λ/L=0.5   *Fn=0.18, λ/L=0.8*   *Fn=0.18, λ/L=1.0*

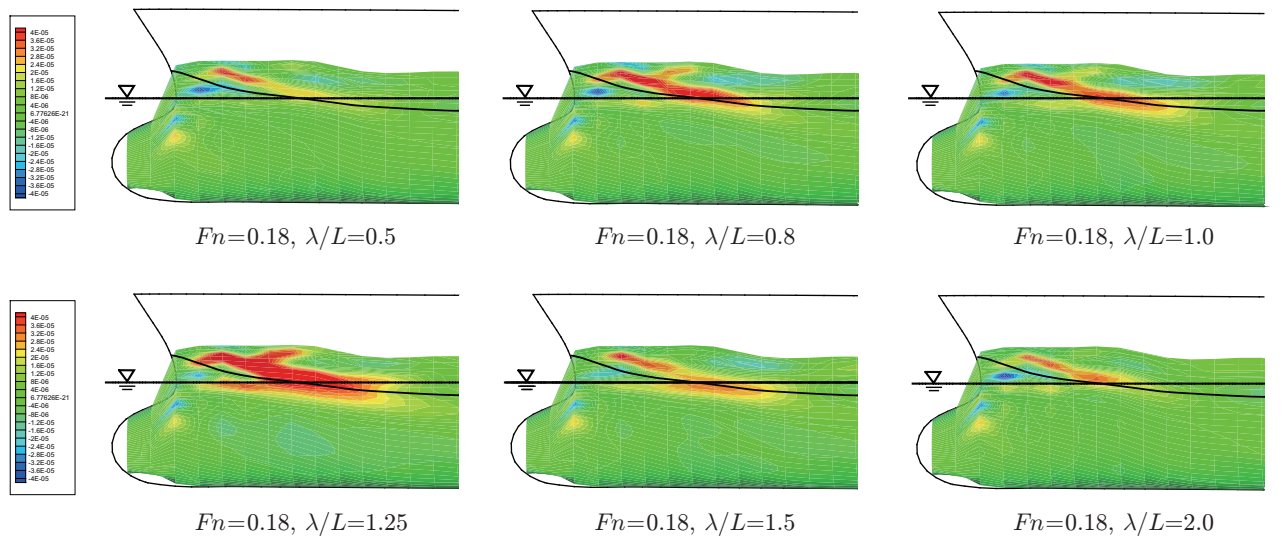*Fn=0.18, λ/L=1.25*   *Fn=0.18, λ/L=1.5*   *Fn=0.18, λ/L=2.0*

Fig. 4 Contour map of added-pressure force in the longitudinal direction at $F_n = 0.18$ and $\chi = 180$ deg.

The results obtained by using the analysis described above are shown in Fig. 4 for head waves of $\lambda/L = 0.5$, 0.8, 1.0, 1.25, 1.5, and 2.0. In these figures, the distribution of added-pressure force acting in the x-direction is displayed only in the bow region, because the dominant contribution is found to exist only in this region, and also both still waterline and steady wave profile on the ship-hull surface at steady translation at $Fn = 0.18$ are shown with black solid lines. We can clearly see from this figure that the dominant added resistance is caused from the values above the still waterline, particularly around (or we may say above) the steady wave profile on the ship-hull surface.

Once the distribution of second-order time-averaged force would be integrated over the wetted surface of a ship according to Eq. (3), the result must be the same as the added resistance measured directly by a dynamometer. The result of this confirmation is shown in Fig. 5. The inverse triangle symbols in red color indicate the results after integration of the added-pressure force distribution, which are in fairly good agreement with the values of the added resistance measured directly by a dynamometer in 2012 (open square symbols) and in 2018 (open triangle symbols). This result may imply that the second and third terms in Eq. (2) are relatively very small.

Regarding the results by numerical computation, the solid line shows the result of EUT, and the green-color circles shows the results computed by CFD (FINE/Marine) at $\lambda/L = 0.5$, 0.8, 1.0, 1.2, 1.5, and 2.0. The agreement with CFD results is also remarkable,
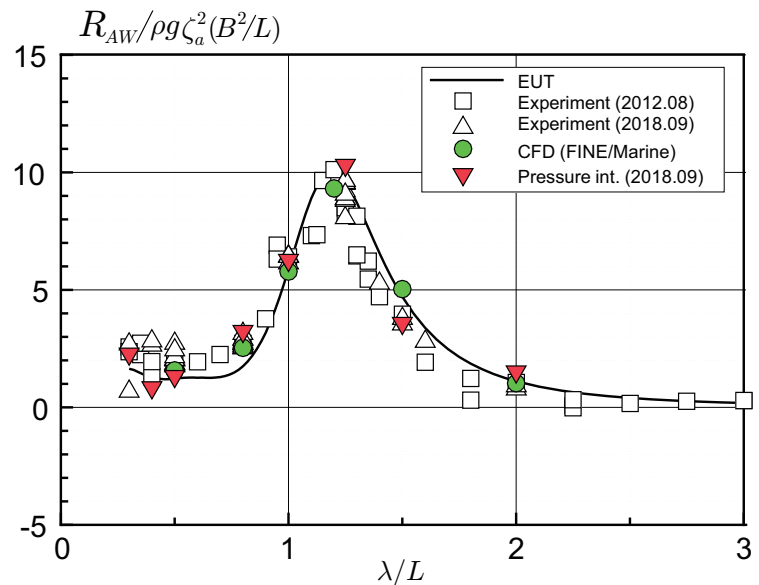

Fig. 5 Comparison of added resistance on RIOS bulk carrier model among direct measurement, pressure integration, numerical computation at $Fn = 0.18$ and $\chi = 180$ deg.

and thus we are going to study the nonlinear nature in the added resistance around the free surface through comparison of the time history of the pressure between experimental measurement and CFD numerical computation.

6 CONCLUSION

Measurement of the spatial distribution of unsteady pressure has been newly conducted in terms of 333 FBG pressure sensors including 70 sensors above the still waterline, from which the distribution of second-order added pressure in connection with the added resistance has been obtained. It was visually shown that the dominant added-pressure force in waves exists around (especially above) the steady wave profile on the ship-hull surface in the bow region. Furthermore, it was confirmed that the integrated value of the distribution of added-pressure force over the whole wetted surface of the ship model is in fairly good agreement with the added resistance measured directly by a dynamometer and also with computed values by CFD method.

REFERENCES

1) Iwashita, H. and Kashiwagi, M.: An Innovative EFD for Studying Ship Seakeeping, Proceedings of 33rd IWWWFB (Guidel-Plages, France), pp. 85-88, 2018.

2) Iwashita, H., Kashiwagi, M., Ito, Y., Seki, Y., Yoshida, J., Wakahara, M.: Calculation of Ship Seakeeping in Low-Speed/Low-Frequency Range by Frequency-Domain Rankine Panel Methods (in Japanese), Journal of The Japan Society of Naval Architects and Ocean Engineers, No.24, pp. 129-146, 2017.

3) Kashiwagi, M.: Prediction of Surge and its Effects on Added Resistance by Means of the Enhanced Unified Theory, Transactions of the West-Japan Society of Naval Architects, No.89, pp. 77-89, 1995.

4) Iwashita, H.: On Numerical Treatments of the Infinite Condition in the Frequency-Domain Rankine Panel Method (in Japanese), Journal of The Japan Society of Naval Architects and Ocean Engineers, No.24, pp. 105-127, 2017.